Reddy, J. N., Romanoff, J., & Loya, J. A. (2016). Nonlinear finite element analysis of functionally graded circular plates with modified couple stress theory. European Journal of Mechanics - A/Solids, 56, 92-104.

DOI: https://doi.org/10.1016/j.euromechsol.2015.11.001

Nonlinear Finite Element Analysis of Functionally Graded Circular Plates with Modified Couple StressTheory

J. N. Reddy, Jani Romanoff, and Jose Antonio Loya

September 2014; Revised: January 2015

Nonlinear Finite Element Analysis of Functionally Graded Circular Plates with Modified Couple StressTheory

J. N. Reddy[1,a], Jani Romanoff[2], and Jose Antonio Loya[3]

[1]Department of Mechanical Engineering, Texas A&M University,
College Station, TX 77843-3123, USA

[2]Department of Solid Mechanics, Aalto University, Finland

[3]Department of Continuum Mechanics and Structural Analysis
University Carlos III of Madrid, Spain

[a]Corresponding author;*e-mail*: jnreddy@tamu.edu

Abstract

Finite element models of microstructure-dependent nonlinear theories for axisymmetric bending of circular plates, which accounts for through-thickness power-law variation of a two-constituent material, the von Kármán nonlinearity, and the strain gradient effects are developed for the classical and first-order theory kinematics. The strain gradient effects are included through the modified couple stress theory that contains a single material length scale parameter which can capture the size effect in a functionally graded material plate. The developed finite element models are used to determine the effect of the geometric nonlinearity, power-law index, and microstructure-dependent constitutive relations on the bending response of functionally graded circular plates.

Keywords. Circular plates; finite element analysis; classical plate theory; first-order plate theory; functionally graded materials; modified couple stress theory; von Kármán nonlinearity.

1 Background

1.1 Microstructural Effects

In recent years a number of models have been derived to include microstructural length scales into the continuum description of beams and plates. Such models are useful in determining the structural response of micro and nano devices made of a variety of new materials that require the consideration of small material length scales over which the neighboring secondary constituents interact, especially when the spatial resolution is comparable to the size of the secondary constituents. Examples of such materials are provided by nematic elastomers and carbon nanotube composites [1] and environment resistent coatings made of CNT reinforced materials [2, 3].

Theories that account for microstructural length scales are the modified couple stress theory of Mindlin [4], Koiter [5], and Toupin [6] and the strain gradient theory of [7]–[9]. A more complete review of the early developments can be found in the work of Srinivasa and Reddy [10]. The strain gradient theory is a more general form of the modified couple

stress theory and the relationship between the modified couple stress theory and the strain gradient theory can be found in the recent work of Reddy and Srinivasa [11].

A number of investigators exploited the modified couple stress theory to model size-effects in homogeneous micro and nano beam and plate structures. Park and Gao [12, 13] investigated analytically the bending problem of a EulerBernoulli beam while Ma et al. [14]–[16] studied bending of beams using shear deformation theories and the modified couples stress model of Yang et al. [17]. Abdi et al. [18] examined the pull-in instability of an electrostatic cantilever nanobeam, Akgöz and Civalek [19] studied analytically the buckling problem of an axially loaded microbeam, Rahaeifard et al. [20] considered the deflection and static pull-in voltage of microcantilevers, and Ansari et al. [21] examined analytically the free vibration response of a Timoshenko graded microbeam. All of the papers cited previously did not account for the geometric nonlinearity. Xia et al. [22] investigated analytically the bending, post-buckling and free vibration behaviors of microbeams while accounting for the von Kármán nonlinear strains.

1.2 Functionally graded materials

The last two decades have witnessed investigators exploring the possibility of using functionally graded materials (FGMs) as a promising alternative to conventional homogenous coatings (see Koizumi [23] and Erdogan [24]). FGMs comprise of at least two constituents that are synthesized in such a way that the volume fractions of the constituents vary continuously along any desired spatial direction, resulting in materials having smooth variation of mechanical properties. Such property enhancements endow FGMs with material properties such as the resilience to fracture. FGMs promise attractive applications in a wide variety of wear coating and thermal shielding problems such as gears, cams, cutting tools, high temperature chambers, furnace liners, turbines, micro-electronics and space structures (see, for example, Reddy and his colleagues [25]–[29] for the analysis of through-thickness, two-constituent FGM beams and plates).

The vast majority of two-constituent FGM studies employed either a power-law or exponential distribution of the materials. In the power-law model, which is more commonly used in bending, vibration, and buckling studies, a typical material property $\mathcal{P}$ is assumed to vary through the thickness according to the formula (see [25]–[29])

$$\mathcal{P}(z,T) = [\mathcal{P}_1(T) - \mathcal{P}_2(T)]\, f(z) + \mathcal{P}_2(T), \quad f(z) = \left(\frac{1}{2} + \frac{z}{h}\right)^n \tag{1}$$

where $\mathcal{P}_1$ and $\mathcal{P}_2$ are the material properties of the top (material 1) and bottom (material 2) faces of the beam or plate, respectively, n is the volume fraction exponent, and T is the temperature (i.e., the material properties can be possibly function of temperature). The exponential model, which is often employed in fracture studies, is based on the formula (see [30, 31])

$$\mathcal{P}(z,T) = \mathcal{P}_1(T)\, \exp\left[-\alpha\left(\frac{1}{2} - \frac{z}{h}\right)\right], \quad \alpha = \log\left(\frac{\mathcal{P}_1(T)}{\mathcal{P}_2(T)}\right) \tag{2}$$

With the progress of technology and fast growth of the use of nanostructures, FGMs have found potential applications in micro and nano scale in the form of shape memory

alloy thin films (see Lü et al. [32]), atomic force microscopes (AFMs) (see Kahrobaiyan et al. [33]), electrically actuated actuators (see Zhang and Fu [34]), and microswitches (see Shariat et al. [35]), to name a few. Few researchers investigated the response of functionally graded micro and nanobeams using modified couple stress or strain gradient theories. Reddy and his colleagues [36]–[43] studied bending, vibration, and buckling of functionally graded Euler-Bernoulli and Timoshenko beams. Simsek and Reddy [39, 40] studied analytically the bending and vibration behaviors of graded microbeams using classical and higher-order beam theories along with the modified couple stress theory to model size-effects. Arbind and Reddy [38] and Arbind, Reddy, and Srinivasa [43] accounted for the von Kármán nonlinear strains to develop nonlinear finite element models for functionally graded Euler-Bernoulli and Timoshenko beams. The von Kármán nonlinearity may have significant contribution to the response of micro- and nano-scale devices such as biosensors and atomic force microscopes (see, for example, Li et al. [44], Pei, Tian, and Thundat [45], and Reddy, El-Borgi, and Romanoff [46]).

1.3 Present Study

A review of literature shows that there are no studies that report nonlinear axisymmetric bending of FGM circular plates with microstructural length scale effects. In particular, no finite element analysis of nonlinear bending of circular plates with modified couple stress theory have been reported. The present paper fills this void in the literature. The objective of the current paper is to develop finite element models of the classical and first-order plate theories for axisymmetric bending of circular plates, accounting for through-thickness power-law variation of a two-constituent material, modified couple stress theory, and the von Kármán nonlinear strains (see Reddy and Berry [37] for the theoretical developments). Since nanoscale devices may involve circular plate elements that may be functionally graded and undergo moderately large rotations, the newly developed finite element models can be used to determine the size effects in functionally graded micro circular plates. Moreover, the bending-extensional coupling is captured through the von Kármán nonlinear strains.

2 Constitutive Models

2.1 Material Variation through the Thickness

Consider a two-constituent functionally graded circular plate of outside radius a, inside radius b, and total thickness h. The r-coordinate is taken radially outward from the center the plate, z-coordinate along the thickness (or height) of the plate, and the θ-coordinate is taken along a circumference of the plate. In a general case where applied loads and geometric boundary conditions are not axisymmetric, the displacements (u_r, u_θ, u_z) along the coordinates (r, θ, z) are functions of r, θ, and z coordinates and time t. We assume that the material of the plate is isotropic but varies from one kind of material at the bottom, $z = -h/2$, to another material on the top, $z = h/2$, so that the modulus $E(z)$ and mass density $\rho(z)$ of the material of the plate vary through the plate thickness according to the

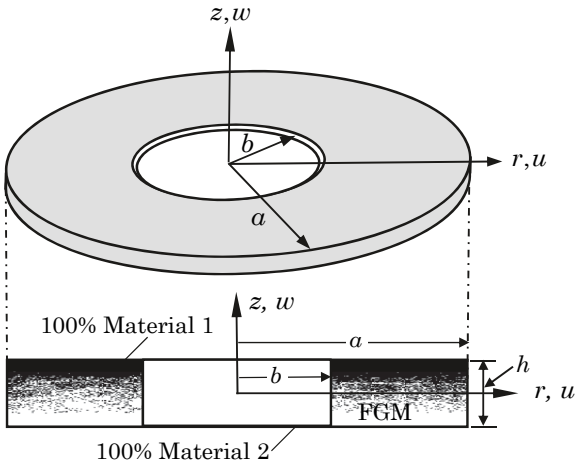

Fig. 1: Geometry and coordinate system for an axisymmetric bending of an FGM circular plate.

power-law (see Fig. 1):

$$E(z) = (E_1 - E_2)\, f(z) + E_2, \quad \rho(z) = (\rho_1 - \rho_2)\, f(z) + \rho_2$$
$$f(z) = \left(\frac{1}{2} + \frac{z}{h}\right)^n \tag{3}$$

where the subscripts 1 and 2 on E and ρ refer the the material number and n denotes the volume fraction exponent, called power-law index. Poisson's ratio ν will be assumed to be constant throughout. When $n = 0$, we obtain the single-material plate (with the property of material 1).

2.2 Modified Couple Stress Theory

According to the modified couple stress theory, the strain energy potential of an elastic beam can be expressed as

$$U = \frac{1}{2} \int_b^a \left[\int_{-\frac{h}{2}}^{\frac{h}{2}} (\boldsymbol{\sigma} : \boldsymbol{\varepsilon} + \mathbf{m} : \boldsymbol{\chi})\, dz \right] r dr \tag{4}$$

where a is the outer radius and b is the inner radius of the plate, $\boldsymbol{\sigma}$ is the Cauchy stress tensor, $\boldsymbol{\varepsilon}$ is the simplified Green–Lagrange strain tensor (as will be discussed in the coming sections), $\mathbf{m}$ is the deviatoric part of the symmetric couple stress tensor, $\boldsymbol{\varepsilon}$ is the von Kármán strain tensor, and $\boldsymbol{\chi}$ is the symmetric curvature tensor

$$\boldsymbol{\chi} = \frac{1}{2} \left[\boldsymbol{\nabla\omega} + (\boldsymbol{\nabla\omega})^{\mathrm{T}} \right] \tag{5}$$

Here $\boldsymbol{\omega}$ denotes the rotation vector

$$\boldsymbol{\omega} = \frac{1}{2}\boldsymbol{\nabla} \times \mathbf{u} \tag{6}$$

where $\mathbf{u}$ is the displacement vector.

The components of the von Kármán strain tensor in cylindrical coordinate system for the axisymmetric case (i.e., independent of θ) are given by (see Reddy[47]–[50])

$$\begin{aligned} \varepsilon_{rr} &= \frac{\partial u_r}{\partial r} + \frac{1}{2}\left(\frac{\partial u_z}{\partial r}\right)^2 \\ \varepsilon_{rz} &= \frac{1}{2}\left(\frac{\partial u_r}{\partial z} + \frac{\partial u_z}{\partial r} + \frac{\partial u_z}{\partial r}\frac{\partial u_z}{\partial z}\right) \\ \varepsilon_{\theta\theta} &= \frac{u_r}{r}, \quad \varepsilon_{zz} = \frac{\partial u_z}{\partial z} \end{aligned} \tag{7}$$

where (u_r, u_z) denote the total displacements along the (r, z) coordinates ($u_\theta = 0$). The only nonzero component of the rotation vector is

$$\omega_\theta = \frac{1}{2}\left(\frac{\partial u_r}{\partial z} - \frac{\partial u_z}{\partial r}\right) \tag{8}$$

Hence, the nonzero components of the curvature tensor are

$$\chi_{r\theta} = \frac{1}{2}\left(\frac{\partial \omega_\theta}{\partial r} - \frac{\omega_\theta}{r}\right), \quad \chi_{z\theta} = \frac{1}{2}\frac{\partial \omega_\theta}{\partial z} \tag{9}$$

3 Classical Plate Theory

3.1 Displacements and Strains

The total displacements (u_r, u_θ, u_z) along the three coordinate directions (r, θ, z), as implied by the Love–Kirchhoff hypothesis for plates, which is the same as the Euler–Bernoulli hypothesis for beams, are assumed in the form

$$\mathbf{u} = u_r\,\hat{\mathbf{e}}_r + u_z\,\hat{\mathbf{e}}_z; \quad u_r(r,z) = u(r) - z\frac{dw}{dr}, \quad u_\theta = 0, \quad u_z(r,z) = w(r) \tag{10}$$

where u is the radial displacement and w is the transverse deflection of the point $(r, 0)$ on the midplane of the plate. The displacement field in Eq. (10) is based on the Kirchhoff hypothesis that straight lines normal to the midplane before deformation remain (1) inextensible, (2) straight, and (3) normal to the midsurface after deformation. The Kirchhoff hypothesis amount to neglecting both transverse shear and transverse normal effects, that is, deformation is due entirely to bending and inplane stretching.

The von Kármán strains in (7) for the classical plate theory take the form

$$\varepsilon_{rr} = \varepsilon_{rr}^{(0)} + z\varepsilon_{rr}^{(1)}, \quad \varepsilon_{\theta\theta} = \varepsilon_{\theta\theta}^{(0)} + z\varepsilon_{\theta\theta}^{(1)} \tag{11}$$

where

$$\begin{aligned} \varepsilon_{rr}^{(0)} &= \frac{du}{dr} + \frac{1}{2}\left(\frac{dw}{dr}\right)^2, \qquad & \varepsilon_{rr}^{(1)} &= -\frac{d^2w}{dr^2} \\ \varepsilon_{\theta\theta}^{(0)} &= \frac{u}{r}, & \varepsilon_{\theta\theta}^{(1)} &= -\frac{1}{r}\frac{dw}{dr} \end{aligned} \tag{12}$$

The rotation and curvature components are

$$\begin{aligned} \omega_\theta &= \frac{1}{2}\left(\frac{du_r}{dz} - \frac{du_z}{dr}\right) = -\frac{dw}{dr} \\ \chi_{r\theta} &= \frac{1}{2}\left(\frac{d\omega_\theta}{dr} - \frac{\omega_\theta}{r}\right) = \frac{1}{2}\left(-\frac{d^2w}{dr^2} + \frac{1}{r}\frac{dw}{dr}\right) \end{aligned} \tag{13}$$

3.2 Equations of Equilibrium

The principle of virtual displacements is used to develop the weak forms and derive the equations of equilibrium. We have,

$$\begin{aligned} 0 &= \int_b^a \int_{-\frac{h}{2}}^{\frac{h}{2}} \left(\sigma_{rr}\,\delta\varepsilon_{rr} + \sigma_{\theta\theta}\,\delta\varepsilon_{\theta\theta} + 2m_{r\theta}\delta\chi_{r\theta}\right) r\,dz\,dr - \int_b^a q\,\delta u_z(r, \frac{h}{2})\,r\,dr \\ 0 &= \int_b^a \Bigg[N_{rr}\left(\frac{d\delta u}{dr} + \frac{dw}{dr}\frac{d\delta w}{dr}\right) + N_{\theta\theta}\left(\frac{\delta u}{r}\right) - M_{rr}\frac{d^2\delta w}{dr^2} \\ &\qquad - \frac{1}{r}M_{\theta\theta}\frac{d\delta w}{dr} + P_{r\theta}\left(-\frac{d^2\delta w}{dr^2} + \frac{1}{r}\frac{d\delta w}{dr}\right) - q\delta w\Bigg] r\,dr\,dt \end{aligned} \tag{14}$$

where $q = q(r)$ is the distributed transverse load, and $(N_{rr}, N_{\theta\theta})$, $(M_{rr}, M_{\theta\theta})$, and $P_{r\theta}$ are the stress resultants defined by

$$\begin{aligned} N_{rr}(r) &= \int_{-\frac{h}{2}}^{\frac{h}{2}} \sigma_{rr}\,dz, \qquad & N_{\theta\theta}(r) &= \int_{-\frac{h}{2}}^{\frac{h}{2}} \sigma_{\theta\theta}\,dz \\ M_{rr}(r) &= \int_{-\frac{h}{2}}^{\frac{h}{2}} \sigma_{rr} z\,dz, & M_{\theta\theta}(r) &= \int_{-\frac{h}{2}}^{\frac{h}{2}} \sigma_{rr} z\,dz \\ P_{r\theta}(r) &= \int_{-\frac{h}{2}}^{\frac{h}{2}} m_{r\theta}\,dz \end{aligned} \tag{15}$$

The equations of equilibrium of the classical plate theory are

$$\frac{1}{r}\left[\frac{d}{dr}\left(rN_{rr}\right) - N_{\theta\theta}\right] = 0 \tag{16}$$

$$\frac{1}{r}\left[\frac{d}{dr}\left(rV_r\right) + \frac{d^2}{dr^2}\left(rP_{r\theta}\right) + \frac{dP_{r\theta}}{dr}\right] + q = 0 \tag{17}$$

where V_r is the effective transverse shear force acting on the rz-plane

$$V_r = Q_r + N_{rr}\frac{dw}{dr} = \frac{1}{r}\left[\frac{d}{dr}\left(rM_{rr}\right) - M_{\theta\theta} + rN_{rr}\frac{dw}{dr}\right] \tag{18}$$

The boundary conditions involve specifying one element of each of the following pairs:

$$\begin{aligned} u \quad &\text{or} \quad rN_{rr} \\ w \quad &\text{or} \quad r\left[V_r + \frac{\partial}{\partial r}\left(rP_{r\theta}\right) + P_{r\theta}\right] \equiv r\hat{V}_r \\ -\frac{dw}{dr} \quad &\text{or} \quad rM_{rr} + rP_{r\theta} \equiv r\hat{M}_{rr} \end{aligned} \tag{19}$$

4 First-Order Theory

4.1 Displacements and Strains

The *first order shear deformation plate theory* (FSDT) (see Reddy [**?**]–[**?**]) is the simplest theory that accounts for nonzero transverse shear strain. It is based on the displacement field

$$\mathbf{u} = u_r\,\hat{\mathbf{e}}_r + u_z\,\hat{\mathbf{e}}_z, \quad u_r(r,z) = u(r) + z\phi(r), \quad u_z(r,z) = w(r) \tag{20}$$

where ϕ denotes rotation of a transverse normal in the plane θ =constant. The first-order theory includes a constant state of transverse shear strain with respect to the thickness coordinate, and hence, requires the use of a shear correction factor, which depend not only on the material and geometric parameters but also on the loading and boundary conditions.

The nonzero von Kármán strains of the theory are

$$\varepsilon_{rr} = \varepsilon_{rr}^{(0)} + z\varepsilon_{rr}^{(1)}, \quad \varepsilon_{\theta\theta} = \varepsilon_{\theta\theta}^{(0)} + z\varepsilon_{\theta\theta}^{(1)}, \quad \varepsilon_{rz} = \varepsilon_{rz}^{(0)} \tag{21}$$

where

$$\begin{aligned} \varepsilon_{rr}^{(0)} &= \frac{du}{dr} + \frac{1}{2}\left(\frac{dw}{dr}\right)^2, \qquad \varepsilon_{rr}^{(1)} = \frac{d\phi}{dr} \\ \varepsilon_{\theta\theta}^{(0)} &= \frac{u}{r}, \qquad \varepsilon_{\theta\theta}^{(1)} = \frac{\phi}{r}, \qquad 2\varepsilon_{rz}^{(0)} = \phi + \frac{dw}{dr} \end{aligned} \tag{22}$$

The rotation and curvature components are

$$\begin{aligned} \omega_\theta &= \frac{1}{2}\left(\frac{du_r}{dz} - \frac{du_z}{dr}\right) = \frac{1}{2}\left(\phi - \frac{dw}{dr}\right) \\ \chi_{r\theta} &= \frac{1}{2}\left(\frac{d\omega_\theta}{dr} - \frac{\omega_\theta}{r}\right) = \frac{1}{4}\left[\frac{d\phi}{dr} - \frac{1}{r}\phi - \left(\frac{d^2w}{dr^2} - \frac{1}{r}\frac{dw}{dr}\right)\right] \end{aligned} \tag{23}$$

4.2 Equations of Equilibrium

The principle of virtual displacements for the first-order theory takes the form

$$\begin{aligned} 0 &= \int_b^a \int_{-\frac{h}{2}}^{\frac{h}{2}} \left(\sigma_{rr}\,\delta\varepsilon_{rr} + \sigma_{\theta\theta}\,\delta\varepsilon_{\theta\theta} + 2K_s\sigma_{rz}\,\delta\varepsilon_{rz} + 2m_{r\theta}\delta\chi_{r\theta}\right) r\,dz\,dr \\ &= \int_b^a \left\{ N_{rr}\left(\frac{d\delta u}{dr} + \frac{dw}{dr}\frac{d\delta w}{dr}\right) + N_{\theta\theta}\left(\frac{\delta u}{r}\right) + M_{rr}\frac{d\delta\phi}{dr} + \frac{1}{r}M_{\theta\theta}\delta\phi - q\delta w \right. \\ &\qquad \left. + Q_r\left(\delta\phi + \frac{d\delta w}{dr}\right) + \frac{1}{2}P_{r\theta}\left[\frac{d\delta\phi}{dr} - \frac{1}{r}\delta\phi - \left(\frac{d^2\delta w}{dr^2} - \frac{1}{r}\frac{d\delta w}{dr}\right)\right]\right\} r\,dr \end{aligned} \tag{24}$$

where the shear force Q_r is defined by

$$Q_r = K_s \int_{-\frac{h}{2}}^{\frac{h}{2}} \sigma_{rz}\,dz \tag{25}$$

and K_s denotes the shear correction factor.

The governing equations of motion of the first-order theory are

$$\frac{1}{r}\left[\frac{d}{dr}\left(rN_{rr}\right) - N_{\theta\theta}\right] = 0 \tag{26}$$

$$\frac{1}{r}\frac{d}{dr}\left(rV_r\right) + \frac{1}{2r}\frac{d}{dr}\left[\frac{d}{dr}\left(rP_{r\theta}\right) + P_{r\theta}\right] + q = 0 \tag{27}$$

$$\frac{1}{r}\left[\frac{d}{dr}\left(rM_{rr}\right) - M_{\theta\theta} + \frac{1}{2}\frac{d}{dr}\left(rP_{r\theta}\right) + \frac{1}{2}P_{r\theta}\right] - Q_r = 0 \tag{28}$$

where

$$V_r = Q_r + N_{rr}\frac{\partial w}{\partial r} \tag{29}$$

The boundary conditions involve specifying one element of each of the following pairs:

$$\begin{aligned} u \quad &\text{or} \quad rN_{rr} \\ w \quad &\text{or} \quad rV_r + \frac{1}{2}\left[\frac{d}{dr}\left(rP_{r\theta}\right) + P_{r\theta}\right] \equiv r\bar{V}_r \\ -\frac{dw}{dr} \quad &\text{or} \quad -\tfrac{1}{2}rP_{r\theta} \equiv r\mathcal{M} \\ \phi \quad &\text{or} \quad rM_{rr} + \tfrac{1}{2}rP_{r\theta} \equiv r\bar{M}_{rr} \end{aligned} \tag{30}$$

5 Plate Constitutive Relations

5.1 Stress–strain relations

For a two-constituent functionally graded linear elastic material, the stress-strain relations are

$$\left\{\begin{array}{c} \sigma_{rr} \\ \sigma_{\theta\theta} \\ \sigma_{rz} \end{array}\right\} = \frac{E(z)}{1-\nu^2}\left[\begin{array}{ccc} 1 & \nu & 0 \\ \nu & 1 & 0 \\ 0 & 0 & \frac{1-\nu}{2} \end{array}\right]\left\{\begin{array}{c} \varepsilon_{rr} \\ \varepsilon_{\theta\theta} \\ 2\varepsilon_{rz} \end{array}\right\} \tag{31}$$

where E varies with z according to Eq. (3) and ν is a constant. The modified couple stress constitutive relations is [4]

$$m_{r\theta} = 2G\ell^2\,\chi_{r\theta} \tag{32}$$

where ℓ is the length scale parameter and G is the shear modulus [$G = 0.5E/(1+\nu)$]. The stress resultants in the two theories can be expressed in terms of the displacements, as given in the next two subsections.

5.2 Classical plate theory

The stress resultants of the classical plate theory are related to the displacements (u, w) according to the relations

$$\begin{aligned}
N_{rr} &= \int_{-\frac{h}{2}}^{\frac{h}{2}} \sigma_{rr}\,dz = A\left[\frac{du}{dr} + \frac{1}{2}\left(\frac{dw}{dr}\right)^2 + \nu\frac{u}{r}\right] - B\left(\frac{d^2w}{dr^2} + \frac{\nu}{r}\frac{dw}{dr}\right)\\
N_{\theta\theta} &= \int_{-\frac{h}{2}}^{\frac{h}{2}} \sigma_{\theta\theta}\,dz = A\left[\frac{u}{r} + \nu\frac{du}{dr} + \frac{\nu}{2}\left(\frac{dw}{dr}\right)^2\right] - B\left(\nu\frac{d^2w}{dr^2} + \frac{1}{r}\frac{dw}{dr}\right)\\
M_{rr} &= \int_{-\frac{h}{2}}^{\frac{h}{2}} \sigma_{rr} z\;dz = B\left[\frac{du}{dr} + \frac{1}{2}\left(\frac{dw}{dr}\right)^2 + \nu\frac{u}{r}\right] - D\left(\frac{d^2w}{dr^2} + \frac{\nu}{r}\frac{dw}{dr}\right)\\
M_{\theta\theta} &= \int_{-\frac{h}{2}}^{\frac{h}{2}} \sigma_{\theta\theta} z\;dz = B\left[\frac{u}{r} + \nu\frac{du}{dr} + \frac{\nu}{2}\left(\frac{dw}{dr}\right)^2\right] - D\left(\nu\frac{d^2w}{dr^2} + \frac{1}{r}\frac{dw}{dr}\right)\\
P_{r\theta} &= \int_{-\frac{h}{2}}^{\frac{h}{2}} m_{r\theta}\;dz = S_{r\theta}\left(-\frac{d^2w}{dr^2} + \frac{1}{r}\frac{dw}{dr}\right)
\end{aligned} \tag{33}$$

where A, B, D, and $S_{r\theta}$ are the extensional, extensional-bending, bending, and shear stiffness coefficients

$$\begin{aligned}
A &= \frac{1}{(1-\nu^2)}\int_{-\frac{h}{2}}^{\frac{h}{2}} E(z)\,dz, \qquad B = \frac{1}{(1-\nu^2)}\int_{-\frac{h}{2}}^{\frac{h}{2}} E(z) z\,dz\\
D &= \frac{1}{(1-\nu^2)}\int_{-\frac{h}{2}}^{\frac{h}{2}} E(z) z^2\,dz, \quad S_{r\theta} = \frac{\ell^2}{2(1+\nu)}\int_{-\frac{h}{2}}^{\frac{h}{2}} E(z)\,dz
\end{aligned} \tag{34}$$

Using the power-law in Eq. (3), we obtain

$$\begin{aligned}
A &= \frac{E_2 h}{1-\nu^2}\frac{M+n}{1+n}, \quad S_{r\theta} = \frac{E_2 h\ell^2}{2(1+\nu)}\frac{M+n}{1+n}\\
B &= \frac{E_2 h^2}{2(1-\nu^2)}\frac{n(M-1)}{(1+n)(2+n)}, \quad M = \frac{E_1}{E_2}\\
D &= \frac{E_2 h^3}{12(1-\nu^2)}\left[\frac{(6+3n+3n^2)M + (8n+3n^2+n^3)}{6+11n+6n^2+n^3}\right]
\end{aligned} \tag{35}$$

5.3 First-order plate theory

The stress resultants in the first-order plate theory can be expressed in terms of the generalized displacements (u, w, ϕ) as

$$
\begin{aligned}
N_{rr} &= \int_{-\frac{h}{2}}^{\frac{h}{2}} \sigma_{rr}\, dz = A\left[\frac{du}{dr} + \frac{1}{2}\left(\frac{dw}{dr}\right)^2 + \nu\frac{u}{r}\right] + B\left(\frac{d\phi}{dr} + \frac{\nu}{r}\phi\right) \\
N_{\theta\theta} &= \int_{-\frac{h}{2}}^{\frac{h}{2}} \sigma_{\theta\theta}\, dz = A\left[\frac{u}{r} + \nu\frac{du}{dr} + \frac{\nu}{2}\left(\frac{dw}{dr}\right)^2\right] + B\left(\nu\frac{d\phi}{dr} + \frac{1}{r}\,\phi\right) \\
M_{rr} &= \int_{-\frac{h}{2}}^{\frac{h}{2}} \sigma_{rr} z\; dz = B\left[\frac{du}{dr} + \frac{1}{2}\left(\frac{dw}{dr}\right)^2 + \nu\frac{u}{r}\right] + D\left(\frac{d\phi}{dr} + \frac{\nu}{r}\,\phi\right) \qquad (36) \\
M_{\theta\theta} &= \int_{-\frac{h}{2}}^{\frac{h}{2}} \sigma_{\theta\theta} z\; dz = B\left[\frac{u}{r} + \nu\frac{du}{dr} + \frac{\nu}{2}\left(\frac{dw}{dr}\right)^2\right] + D\left(\nu\frac{d\phi}{dr} + \frac{1}{r}\,\phi\right) \\
Q_r &= \int_{-\frac{h}{2}}^{\frac{h}{2}} \sigma_{rz}\; dz = K_s S_{rz}\left(\phi + \frac{dw}{dr}\right) \\
P_{r\theta} &= \int_{-\frac{h}{2}}^{\frac{h}{2}} m_{r\theta}\, dz = \frac{1}{2} S_{r\theta}\left[\frac{d\phi}{dr} - \frac{d^2 w}{dr^2} - \frac{1}{r}\left(\phi - \frac{dw}{dr}\right)\right] \qquad (37)
\end{aligned}
$$

where A, B, D, and $S_{rz} = S_{r\theta}$ are the stiffness coefficients defined in Eqs. (34) and (35).

6 Finite Element Models

6.1 Classical plate theory

The statement in Eq. (14) is equivalent to the following two statements over a typical finite element $\Omega^e = (r_a, r_b)$:

$$
\begin{aligned}
0 &= \int_{r_a}^{r_b} \left[N_{rr}\frac{d\delta u}{dr} + N_{\theta\theta}\left(\frac{\delta u}{r}\right)\right] r\, dr - Q_1 \delta u(r_a) - Q_4 \delta u(r_b) \qquad (38) \\
0 &= \int_{r_a}^{r_b} \Bigg[N_{rr}\frac{dw}{dr}\frac{d\delta w}{dr} - M_{rr}\frac{d^2\delta w}{dr^2} \\
&\qquad - \frac{1}{r}M_{\theta\theta}\frac{d\delta w}{dr} + P_{r\theta}\left(-\frac{d^2\delta w}{dr^2} + \frac{1}{r}\frac{d\delta w}{dr}\right) - q\delta w\Bigg] r\, dr \\
&\quad - \left[Q_2\delta w(r_a) + Q_5\delta w(r_b) + Q_3\delta\theta(r_a) + Q_6\delta\theta(r_b)\right] \qquad (39)
\end{aligned}
$$

where N_{rr}, $N_{\theta\theta}$, M_{rr}, $M_{\theta\theta}$, and $P_{r\theta}$ are known in terms of u and w through Eqs. (33), θ denotes the slope $\theta = -(dw/dr)$, and Q_i are the generalized forces at the nodes of the

Figure 2

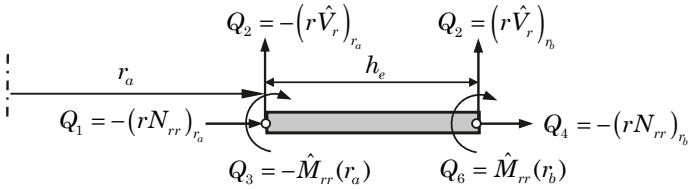

(a) Secondary variables of the classical plate theory element

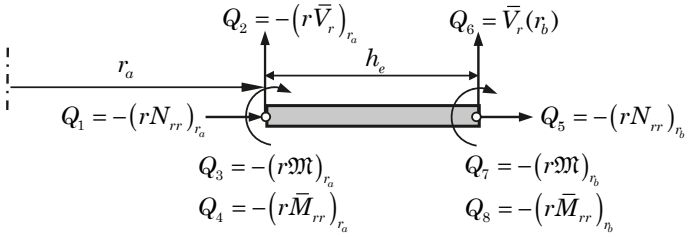

(b) Secondary variables of the first-order plate theory element

Fig. 2: Secondary variables of a typical finite element for (a) classical plate theory and (b) first-order shear deformation plate theory.

element for a circular plate [see Fig. 2(a)]:

$$\begin{aligned} Q_1 &\equiv -\left[rN_{rr}\right]_{r_a}, & Q_4 &\equiv \left[rN_{rr}\right]_{r_b} \\ Q_2 &\equiv -\left[r\hat{V}_r\right]_{r_a}, & Q_5 &\equiv \left[r\hat{V}_r\right]_{r_b} \\ Q_3 &\equiv -\left[r\hat{M}_{rr}\right]_{r_a}, & Q_6 &\equiv \left[r\hat{M}_{rr}\right]_{r_b} \end{aligned} \tag{40}$$

An examination of the boundary conditions in Eq. (19) show that the Lagrange interpolation of u and Hermite interpolation of w is necessary. Let

$$u(r) = \sum_{j=1}^{2} \Delta_j^1 \psi_j(r), \quad w(r) = \sum_{J=1}^{4} \Delta_J^2 \varphi_J(r) \tag{41}$$

where $\psi_j(r)$ are the linear polynomials, $\varphi_J(r)$ are the Hermite cubic polynomials, (Δ_1^1, Δ_2^1) are the nodal values of u at r_a and r_b, respectively, and Δ_J^2 ($J = 1, 2, 3, 4$) are the nodal values associated with w:

$$\Delta_1^2 = w(r_a), \quad \Delta_3^2 = w(r_b), \quad \Delta_2^2 = -\left.\frac{dw}{dr}\right|_{r_a}, \quad \Delta_4^2 = -\left.\frac{dw}{dr}\right|_{r_b} \tag{42}$$

Substitution of the approximations in Eq.(41) into Eqs. (38) and (39), we obtain the

following finite element model:

$$\begin{bmatrix} \mathbf{K}^{11} & \mathbf{K}^{12} \\ \mathbf{K}^{21} & \mathbf{K}^{22} \end{bmatrix} \begin{Bmatrix} \boldsymbol{\Delta}^1 \\ \boldsymbol{\Delta}^2 \end{Bmatrix} = \begin{Bmatrix} \mathbf{F}^1 \\ \mathbf{F}^2 \end{Bmatrix} \tag{43}$$

The stiffness coefficients $K_{ij}^{\alpha\beta}$ and force coefficients F_i^{α} $(\alpha, \beta = 1, 2)$ are defined as follows:

$$\begin{aligned}
K_{ij}^{11} &= \int_{r_a}^{r_b} A \left[\frac{d\psi_i}{dr} \left(\frac{d\psi_j}{dr} + \frac{\nu}{r}\psi_j \right) + \frac{1}{r}\psi_i \left(\frac{1}{r}\psi_j + \nu \frac{d\psi_j}{dr} \right) \right] r dr \\
K_{iJ}^{12} &= \int_{r_a}^{r_b} \left\{ \frac{d\psi_i}{dr} \left[A\frac{1}{2}\frac{dw}{dr}\frac{d\varphi_J}{dr} - B\left(\frac{d^2\varphi_J}{dr^2} + \frac{\nu}{r}\frac{d\varphi_J}{dr} \right) \right] \right. \\
&\qquad \left. + \frac{1}{r}\psi_i \left[\frac{1}{2}A\nu\frac{dw}{dr}\frac{d\varphi_J}{dr} - B\left(\nu\frac{d^2\varphi_J}{dr^2} + \frac{1}{r}\frac{d\varphi_J}{dr} \right) \right] \right\} r dr \\
K_{Ij}^{21} &= \int_{r_a}^{r_b} \left[\left(A\frac{dw}{dr}\frac{d\varphi_I}{dr} - B\frac{d^2\varphi_I}{dr^2} \right) \left(\frac{d\psi_j}{dr} + \frac{\nu}{r}\psi_j \right) \right. \\
&\qquad \left. - B\frac{1}{r}\frac{d\varphi_I}{dr} \left(\frac{1}{r}\psi_j + \nu\frac{d\psi_j}{dr} \right) \right] r dr \\
K_{IJ}^{22} &= \int_{r_a}^{r_b} \left\{ \frac{dw}{dr}\frac{d\varphi_I}{dr} \left[\frac{1}{2}A\frac{dw}{dr}\frac{d\varphi_J}{dr} - B\left(\frac{d^2\varphi_J}{dr^2} + \frac{\nu}{r}\frac{d\varphi_J}{dr} \right) \right] \right. \\
&\quad - \frac{d^2\varphi_I}{dr^2} \left[\frac{1}{2}B\frac{dw}{dr}\frac{d\varphi_J}{dr} - D\left(\frac{d^2\varphi_J}{dr^2} + \frac{\nu}{r}\frac{d\varphi_J}{dr} \right) \right] \\
&\quad - \frac{1}{r}\frac{d\varphi_I}{dr} \left[\frac{1}{2}B\nu\frac{dw}{dr}\frac{d\varphi_J}{dr} - D\left(\nu\frac{d^2\varphi_J}{dr^2} + \frac{1}{r}\frac{d\varphi_J}{dr} \right) \right] \\
&\quad \left. + S_{r\theta} \left(-\frac{d^2\varphi_I}{dr^2} + \frac{1}{r}\frac{d\varphi_I}{dr} \right) \left(-\frac{d^2\varphi_J}{dr^2} + \frac{1}{r}\frac{d\varphi_J}{dr} \right) \right\} r dr \\
F_i^1 &= Q_1\psi_i(r_a) + Q_4\psi_i(r_b) \\
F_I^2 &= \int_{r_a}^{r_b} q\varphi_I \, r dr + Q_2\varphi_I(r_a) + Q_5\varphi_I(r_b) + Q_3 \left[-\frac{d\varphi_I}{dx} \right]_{r_a} + Q_6 \left[-\frac{d\varphi_I}{dx} \right]_{r_b}
\end{aligned} \tag{44}$$

6.2 Firs-order plate theory

The virtual work statement in Eq. (24) is equivalent to the following three statements over a typical finite element $\Omega^e = (r_a, r_b)$:

$$0 = \int_{r_a}^{r_b} \left(N_{rr} \frac{d\delta u}{dr} + N_{\theta\theta} \frac{\delta u}{r} \right) r\, dr - Q_1 \delta u(r_a) - Q_4 \delta u(r_b) \tag{45}$$

$$\begin{aligned} 0 = \int_{r_a}^{r_b} \left[N_{rr} \frac{dw}{dr} \frac{d\delta w}{dr} + Q_r \frac{d\delta w}{dr} + \frac{1}{2} P_{r\theta} \left(-\frac{d^2 \delta w}{dr^2} + \frac{1}{r} \frac{d\delta w}{dr} \right) - q\delta w \right] r\, dr \\ - Q_2 \delta w(r_a) - Q_5 \delta w(r_b) \end{aligned} \tag{46}$$

$$\begin{aligned} 0 = \int_{r_a}^{r_b} \left[M_{rr} \frac{d\delta \phi}{dr} + \frac{1}{r} M_{\theta\theta} \delta\phi + Q_r \delta\phi + \frac{1}{2} P_{r\theta} \left(\frac{d\delta\phi}{dr} + \frac{1}{r} \delta\phi \right) \right] r\, dr \\ - Q_3 \delta\phi(r_a) - Q_6 \delta\phi(r_b) \end{aligned} \tag{47}$$

where N_{rr}, $N_{\theta\theta}$, M_{rr}, $M_{\theta\theta}$, and $P_{r\theta}$ are known in terms of u and w through Eq. (33), and Q_i are the generalized forces at the nodes of the element for a circular plate [see Fig. 2(b)]:

$$\begin{aligned} Q_1 &\equiv -\left[r N_{rr} \right]_{r_a}, & Q_5 &\equiv \left[r N_{rr} \right]_{r_b} \\ Q_2 &\equiv -\left[r \bar{V}_r \right]_{r_a}, & Q_6 &\equiv \left[r \bar{V}_r \right]_{r_b} \\ Q_3 &\equiv -\left[r \mathcal{M} \right]_{r_a}, & Q_7 &\equiv \left[r \mathcal{M} \right]_{r_b} \\ Q_4 &\equiv -\left[r \bar{M}_{rr} \right]_{r_a}, & Q_8 &\equiv \left[r \bar{M}_{rr} \right]_{r_b} \end{aligned} \tag{48}$$

An examination of the boundary conditions in Eq. (30) show that the Lagrange interpolation of (u, ϕ) and Hermite interpolation of w are required. Let

$$u(r) = \sum_{j=1}^{m} U_j \psi_j^{(1)}(r), \quad w(r,t) = \sum_{j=1}^{4} \Delta_j \psi_j^{(2)}(r), \quad \phi(r,t) = \sum_{j=1}^{n} \Phi_j \psi_j^{(3)}(r), \tag{49}$$

where $\psi_j^{(1)}$ and $\psi_j^{(3)}$ are the Lagrange polynomials of different degree used for u and ϕ, respectively, and $\psi_j^{(2)}$ are the Hermite cubic polynomials. Substitution of the approximations in Eq.(49) into Eqs. (45)–(47), we obtain the following finite element model:

$$\begin{bmatrix} \mathbf{K}^{11} & \mathbf{K}^{12} & \mathbf{K}^{13} \\ \mathbf{K}^{21} & \mathbf{K}^{22} & \mathbf{K}^{23} \\ \mathbf{K}^{31} & \mathbf{K}^{32} & \mathbf{K}^{33} \end{bmatrix} \begin{Bmatrix} \mathbf{U} \\ \mathbf{\Delta} \\ \mathbf{\Phi} \end{Bmatrix} = \begin{Bmatrix} \mathbf{F}^1 \\ \mathbf{F}^2 \\ \mathbf{F}^3 \end{Bmatrix} \tag{50}$$

The nonzero mass and stiffness coefficients, $M_{ij}^{\alpha\beta}$ and $K_{ij}^{\alpha\beta}$, and force coefficients F_i^{α}

$(\alpha, \beta = 1, 2, 3)$ are defined as follows:

$$
\begin{aligned}
K_{ij}^{11} &= \int_{r_a}^{r_b} A \left[\frac{d\psi_i^{(1)}}{dr} \left(\frac{d\psi_j^{(1)}}{dr} + \frac{\nu}{r}\psi_j^{(1)} \right) + \frac{1}{r}\psi_i^{(1)} \left(\frac{1}{r}\psi_j^{(1)} + \nu \frac{d\psi_j^{(1)}}{dr} \right) \right] r dr \\
K_{ij}^{12} &= \frac{1}{2} \int_{r_a}^{r_b} A \frac{dw}{dr} \left(\frac{d\psi_i^{(1)}}{dr} + \frac{\nu}{r}\psi_i^{(1)} \right) \frac{d\psi_j^{(2)}}{dr} \, r dr \\
K_{ij}^{21} &= \int_{r_a}^{r_b} A \frac{dw}{dr} \frac{d\psi_i^{(2)}}{dr} \left(\frac{d\psi_j^{(1)}}{dr} + \frac{\nu}{r}\psi_j^{(1)} \right) r dr \\
K_{ij}^{13} &= \int_{r_a}^{r_b} B \left[\frac{d\psi_i^{(1)}}{dr} \left(\frac{d\psi_j^{(3)}}{dr} + \frac{\nu}{r}\psi_j^{(3)} \right) + \frac{1}{r}\psi_i^{(1)} \left(\nu \frac{d\psi_j^{(3)}}{dr} + \frac{1}{r}\psi_j^{(3)} \right) \right] r dr \\
K_{ij}^{22} &= \int_{r_a}^{r_b} \left[\frac{1}{2} A \left(\frac{dw}{dr} \right)^2 \frac{d\psi_i^{(2)}}{dr} \frac{d\psi_j^{(2)}}{dr} + K_s S_{rz} \frac{d\psi_i^{(2)}}{dr} \frac{d\psi_j^{(2)}}{dr} \right. \\
&\quad \left. + \frac{1}{2} S_{r\theta} \left(-\frac{d^2\psi_i^{(2)}}{dr^2} + \frac{1}{r}\frac{d\psi_i^{(2)}}{dr} \right) \left(-\frac{d^2\psi_j^{(2)}}{dr^2} + \frac{1}{r}\frac{d\psi_j^{(2)}}{dr} \right) \right] r dr \\
K_{ij}^{23} &= \int_{r_a}^{r_b} \left[B \frac{dw}{dr} \frac{d\psi_i^{(2)}}{dr} \left(\frac{d\psi_j^{(1)}}{dr} + \frac{\nu}{r}\psi_j^{(1)} \right) + K_s S_{rz} \frac{d\psi_i^{(2)}}{dr} \psi_j^{(3)} \right. \\
&\quad \left. + \frac{1}{4} S_{r\theta} \left(-\frac{d^2\psi_i^{(2)}}{dr^2} + \frac{1}{r}\frac{d\psi_i^{(2)}}{dr} \right) \left(\frac{d\psi_j^{(3)}}{dr} - \frac{1}{r}\psi_j^{(3)} \right) \right] r dr \\
K_{ij}^{31} &= \int_{r_a}^{r_b} B \left[\frac{d\psi_i^{(3)}}{dr} \left(\frac{d\psi_j^{(1)}}{dr} + \frac{\nu}{r}\psi_j^{(1)} \right) + \frac{1}{r}\psi_i^{(3)} \left(\nu \frac{d\psi_j^{(1)}}{dr} + \frac{1}{r}\psi_j^{(1)} \right) \right] r dr \\
K_{ij}^{32} &= \int_{r_a}^{r_b} \left[\frac{1}{2} B \frac{dw}{dr} \left(\frac{d\psi_i^{(3)}}{dr} + \frac{\nu}{r}\psi_i^{(3)} \right) \frac{d\psi_j^{(2)}}{dr} + K_s S_{rz} \psi_i^{(3)} \frac{d\psi_j^{(2)}}{dr} \right. \\
&\quad \left. + \frac{1}{4} S_{r\theta} \left(\frac{d\psi_i^{(3)}}{dr} - \frac{1}{r}\psi_i^{(3)} \right) \left(-\frac{d^2\psi_j^{(2)}}{dr^2} + \frac{1}{r}\frac{d\psi_j^{(2)}}{dr} \right) \right] r dr \\
K_{ij}^{33} &= \int_{r_a}^{r_b} \left\{ D \left[\frac{d\psi_i^{(3)}}{dr} \left(\frac{d\psi_j^{(3)}}{dr} + \frac{\nu}{r}\psi_j^{(3)} \right) + \frac{1}{r}\psi_i^{(3)} \left(\nu \frac{d\psi_j^{(3)}}{dr} + \frac{1}{r}\psi_j^{(3)} \right) \right] \right. \\
&\quad \left. + K_s S_{rz} \psi_i^{(3)} \psi_j^{(3)} + \frac{1}{4} S_{r\theta} \left(\frac{d\psi_i^{(3)}}{dr} - \frac{1}{r}\psi_i^{(3)} \right) \left(\frac{d\psi_j^{(3)}}{dr} - \frac{1}{r}\psi_j^{(3)} \right) \right\} r dr \\
F_i^1 &= Q_1 \psi_i^{(1)}(r_a) + Q_4 \psi_i^{(1)}(r_b), \quad F_i^3 = Q_3 \psi_i^{(3)}(r_a) + Q_6 \psi_i^{(3)}(r_b) \\
F_i^2 &= \int_{r_a}^{r_b} q \psi_i^{(2)} \, r dr + Q_2 \psi_i^{(2)}(r_a) + Q_5 \psi_i^{(2)}(r_b)
\end{aligned}
\tag{51}
$$

6.3 Solution of Nonlinear Equations

6.3.1 Newton's Iteration Procedure

The solution of the nonlinear equations in Eqs. (43) and (50) is discussed here using Newton's iterative procedure. The linearized element equations at the beginning of the rth iteration are of the form

$$\mathbf{T}^e(\boldsymbol{\Delta}^{(r-1)})\delta\boldsymbol{\Delta}^{(r)} = -\mathbf{R}^e(\boldsymbol{\Delta}^{(r-1)}) = (\mathbf{F}^e - \mathbf{K}^e\boldsymbol{\Delta}^e)^{(r-1)} \tag{52}$$

where the tangent stiffness matrix $\mathbf{T}^e$ is calculated using the definition

$$\mathbf{T}^e \equiv \frac{\partial \mathbf{R}^e}{\partial \boldsymbol{\Delta}^e} \quad \text{or} \quad T^e_{ij} \equiv \frac{\partial R^e_i}{\partial \Delta^e_j} \tag{53}$$

The global incremental displacement vector $\delta\mathbf{U}$ at the rth iteration is obtained by solving the assembled equations (after the imposition of the boundary conditions)

$$\delta\mathbf{U} = -[\mathbf{T}(\mathbf{U}^{(r-1)})]^{-1}\mathbf{R}^{(r-1)} \tag{54}$$

and the total solution is computed from

$$\mathbf{U}^{(r)} = \mathbf{U}^{(r-1)} + \delta\mathbf{U} \tag{55}$$

At the beginning of the iteration process, that is, when $r = 1$, solution $\mathbf{U}^{(0)}$ that is consistent with the problem boundary conditions must be assumed. For problems with homogeneous boundary conditions, one may take $\mathbf{U}^{(0)} = \mathbf{0}$ so that the first iteration solution is the linear solution. Using the solution from the $(r-1)$st iteration, we can compute the coefficient matrix $\mathbf{K}^{(r-1)} \equiv \mathbf{K}(\mathbf{U}^{(r-1)})$ and vector $\mathbf{F}^{(r-1)} \equiv \mathbf{F}(\mathbf{U}^{(r-1)})$. The solution at the rth iteration is determined by solving Eq. (54). Once the solution $\mathbf{U}^{(r)}$ is obtained, we check to see if the residual vector

$$\mathbf{R}^{(r)} \equiv \mathbf{K}^{(r)}\mathbf{U}^{(r)} - \mathbf{F}^{(r)} \tag{56}$$

is zero. The magnitude of this residual vector will be small enough if the solution has converged. In other words, we terminate the iteration if the magnitude of the residual vector, measured in a suitable norm, is less than some preselected tolerance ϵ. If the problem data are such that $\mathbf{KU}$ as well as $\mathbf{F}$ are very small, the norm of the residual vector may also be very small even when the solution $\mathbf{U}$ has not converged. Therefore, it is necessary to normalize the residual vector with respect to $\mathbf{F}$. Using the Euclidean norm, we can express the error criterion as

$$\sqrt{\frac{\mathbf{R}^{(r)} \cdot \mathbf{R}^{(r)}}{\mathbf{F}^{(r)} \cdot \mathbf{F}^{(r)}}} \leq \epsilon \tag{57}$$

Alternatively, one may check to see if the normalized difference between solution vectors from two consecutive iterations, measured with the Euclidean norm, is less than a preselected tolerance ϵ:

$$\sqrt{\frac{\Delta\mathbf{U} \cdot \Delta\mathbf{U}}{\mathbf{U}^{(r)} \cdot \mathbf{U}^{(r)}}} = \sqrt{\frac{\sum_{I=1}^{N} |U_I^{(r)} - U_I^{(r-1)}|^2}{\sum_{I=1}^{N} |U_I^{(r)}|^2}} \leq \epsilon \tag{58}$$

where $\Delta\mathbf{U} = \mathbf{U}^{(r)} - \mathbf{U}^{(r-1)}$. Thus, the iteration process is continued until the error criterion inEq. (58) is satisfied. The is is the error criterion used in the present study.

Acceleration of convergence for some types of nonlinearities may be achieved by using a weighted-average of solutions from the last two iterations rather than the solution from the last iteration to evaluate the coefficient matrix:

$$\mathbf{U}^{(r)} = [\mathbf{K}(\bar{\mathbf{U}})]^{-1}\mathbf{F}(\bar{\mathbf{U}}), \quad \bar{\mathbf{U}} \equiv \beta\mathbf{U}^{(r-2)} + (1-\beta)\mathbf{U}^{(r-1)}, \quad 0 \le \beta \le 1 \tag{59}$$

where β is known as the acceleration parameter. The value of β depends on the nature of nonlinearity and the type of problem. Often, one has to play with the value of β to obtain convergence.

For the form of the finite element equations at hand, the tangent stiffness matrix $\mathbf{T}$ is assumed to be of the same form as the direct stiffness matrix $\mathbf{K}$ for each theory. Then the coefficients of the submatrices $\mathbf{T}^{\alpha\beta}$ can be computed using the definition

$$T_{ij}^{\alpha\beta} \equiv \frac{\partial R_i^\alpha}{\partial \Delta_j^\beta} = K_{ij}^{\alpha\beta} + \sum_{k=1}^{n_\gamma} \frac{\partial K_{ik}^{\alpha\gamma}}{\partial \Delta_j^\beta}\Delta_k^\gamma - \frac{\partial F_i^\alpha}{\partial \Delta_j^\beta} \tag{60}$$

6.3.2 Tangent stiffness coefficients for the classical plate theory

The tangent stiffness coefficients for this case are given by

$$\begin{aligned}
&T_{ij}^{11} = K_{ij}^{11}, \quad T_{iJ}^{12} = K_{iJ}^{12} + \int_{r_a}^{r_b} \frac{1}{2}A\frac{d\bar{w}}{dr}\left(\frac{d\psi_i}{dr}\frac{d\varphi_J}{dr} + \frac{\nu}{r}\psi_i\frac{d\varphi_J}{dr}\right) r dr = T_{Ji}^{21}, \quad T_{Ij}^{21} = K_{Ij}^{21},\\
&T_{IJ}^{22} = K_{IJ}^{22} + \int_{r_a}^{r_b}\left[A\left\{\frac{d\varphi_I}{dr}\frac{d\varphi_J}{dr}\left[\left(\frac{d\bar{w}}{dr}\right)^2 + \frac{d\bar{u}}{dr} + \nu\frac{\bar{u}}{r}\right]\right\} - B\frac{d\varphi_I}{dr}\frac{d\varphi_J}{dr}\left(\frac{d^2\bar{w}}{dr^2} + \frac{\nu}{r}\frac{d\bar{w}}{dr}\right)\right.\\
&\qquad\left. - \frac{1}{2}B\frac{d\bar{w}}{dr}\left(\frac{d^2\varphi_I}{dr^2}\frac{d\varphi_J}{dr} + \frac{\nu}{r}\frac{d\varphi_I}{dr}\frac{d\varphi_J}{dr}\right)\right] r dr\\
&= \int_{r_a}^{r_b}\left[A\left\{\frac{d\varphi_I}{dr}\frac{d\varphi_J}{dr}\left[1.5\left(\frac{d\bar{w}}{dr}\right)^2 + \frac{d\bar{u}}{dr} + \nu\frac{\bar{u}}{r}\right]\right\}\right.\\
&\qquad - B\left[\frac{d\varphi_I}{dr}\frac{d\varphi_J}{dr}\left(\frac{d^2\bar{w}}{dr^2} + \frac{3\nu}{r}\frac{d\bar{w}}{dr}\right) + \left(\frac{d^2\varphi_I}{dr^2}\frac{d\varphi_J}{dr} + \frac{d\varphi_I}{dr}\frac{d^2\varphi_J}{dr^2}\right)\frac{d\bar{w}}{dr}\right]\\
&\qquad + D\left[\frac{d^2\varphi_I}{dr^2}\left(\frac{d^2\varphi_J}{dr^2} + \frac{\nu}{r}\frac{d\varphi_J}{dr}\right) + \frac{1}{r}\frac{d\varphi_I}{dr}\left(\nu\frac{d^2\varphi_J}{dr^2} + \frac{1}{r}\frac{d\varphi_J}{dr}\right)\right]\\
&\qquad \left. + S_{r\theta}\left(-\frac{d^2\varphi_I}{dr^2} + \frac{1}{r}\frac{d\varphi_I}{dr}\right)\left(-\frac{d^2\varphi_J}{dr^2} + \frac{1}{r}\frac{d\varphi_J}{dr}\right)\right\} r dr
\end{aligned} \tag{61}$$

where the bar over w and u indicates that they are evaluated using the nodal values from the previous iteration [see Eq. (59)]. The tangent stiffness matrix is symmetric (i.e., $T_{ij}^{\alpha\beta} = T_{ji}^{\beta\alpha}$).

6.3.3 Tangent stiffness coefficients for the first-order plate theory

The tangent stiffness coefficients for the FSDT are given by

$$
\begin{aligned}
&T_{ij}^{11} = K_{ij}^{11}, \quad T_{ij}^{12} = 2K_{ij}^{12}, \quad T_{ij}^{21} = K_{ij}^{21}, \quad T_{ij}^{13} = K_{ij}^{13} \\
&T_{ij}^{31} = K_{ij}^{31} = T_{ji}^{13}, \quad T_{ij}^{23} = K_{ij}^{23}, \quad T_{ij}^{33} = K_{ij}^{33} \\
&T_{ij}^{22} = K_{ij}^{22} + \int_{r_a}^{r_b} \left\{ A\left[\left(\frac{d\bar{w}}{dx} \right)^2 + \frac{d\bar{u}}{dr} + \nu \frac{\bar{u}}{r} \right] + B\left(\frac{d\bar{u}}{dr} + \nu \frac{\bar{u}}{r} \right) \right\} \frac{d\psi_i^{(2)}}{dr} \frac{d\psi_j^{(2)}}{dr} r dr \\
&\quad = \int_{r_a}^{r_b} \left[\left\{ A\left[1.5 \left(\frac{d\bar{w}}{dx} \right)^2 + \frac{d\bar{u}}{dr} + \nu \frac{\bar{u}}{r} \right] + B\left(\frac{d\bar{u}}{dr} + \nu \frac{\bar{u}}{r} \right) \right\} \frac{d\psi_i^{(2)}}{dr} \frac{d\psi_j^{(2)}}{dr} r dr \right. \\
&\qquad \left. + K_s S_{rz} \frac{d\psi_i^{(2)}}{dr} \frac{d\psi_j^{(2)}}{dr} + \frac{1}{2} S_{r\theta} \left(-\frac{d^2\psi_i^{(2)}}{dr^2} + \frac{1}{r} \frac{d\psi_i^{(2)}}{dr} \right) \left(-\frac{d^2\psi_j^{(2)}}{dr^2} + \frac{1}{r} \frac{d\psi_j^{(2)}}{dr} \right) \right] r dr \\
&T_{ij}^{32} = K_{ij}^{32} + \frac{1}{2} \int_{r_a}^{r_b} B \frac{d\bar{w}}{dr} \left(\frac{d\psi_i^{(3)}}{dr} + \frac{\nu}{r} \psi_i^{(3)} \right) \frac{d\psi_j^{(2)}}{dr} r dr \\
&\quad = \int_{r_a}^{r_b} \left[B \frac{d\bar{w}}{dr} \left(\frac{d\psi_i^{(3)}}{dr} + \frac{\nu}{r} \psi_i^{(3)} \right) \frac{d\psi_j^{(2)}}{dr} + K_s S_{rz} \psi_i^{(3)} \frac{d\psi_j^{(2)}}{dr} \right. \\
&\qquad \left. + \frac{1}{4} S_{r\theta} \left(\frac{d\psi_i^{(3)}}{dr} - \frac{1}{r} \psi_i^{(3)} \right) \left(-\frac{d^2\psi_j^{(2)}}{dr^2} + \frac{1}{r} \frac{d\psi_j^{(2)}}{dr} \right) \right] r dr = T_{ji}^{23}
\end{aligned}
\tag{62}
$$

The tangent stiffness matrix of the TBT element is also symmetric.

7 Numerical Results

Here we consider several examples of solid and annular circular plates with clamped and simply supported boundary conditions to determine the parametric effects of the power-law index n and the length scale parameters ℓ [see Eq. (32)] on the nonlinear load-deflection behavior.

The following parameters are used in obtaining the numerical results (no specific units are used) in theexamples:

$$
h = 0.1, \quad L = 10h, \quad \nu = 0.25, \quad E_1 = 10^6, \quad E_2 = 10^5, \quad K_s = 5/6. \tag{63}
$$

Convergence studies were carried out to verify the linear and nonlinear solution of the clamped homogeneous solid circular plates under uniformly distributed transverse load by comparing with the analytical and finite element solutions from Reddy [49, 52]. In all cases, unless stated otherwise, 16 CPT or FSDT elements are used. We note that the CPT element has three $(u, w, -dw/dx)$ while the FSDT element has four $(u, w, -dw/dx, \phi)$ degrees of freedom per node. The difference between the results predicted by the two theories is not significant even for $a/h = 10$ (i.e., the shear deformation effect cannot be distinctly seen in the graphs). Numerical results are presented for various values of the power-law index n. The ratio of the length scale to the thickness of the plate ℓ/h is varied.

These values selected only to determine the parametric effects and they do not necessarily correspond to any specific physical system.

The first example deals with a clamped solid circular plate under uniformly distributed transverse load of intensity q_0. The boundary conditions used in the two theories are as follows:

$$\begin{aligned} \text{CPT:}\ \ & u = \frac{dw}{dx} = 0 \text{ at } r = 0; \quad u = w = \frac{dw}{dx} = 0 \text{ at } r = a \\ \text{FSDT:}\ \ & u = \frac{dw}{dx} = \phi = 0 \text{ at } r = 0; \quad u = w = \frac{dw}{dx} = \phi = 0 \text{ at } r = a \end{aligned} \tag{64}$$

The load steps were of the magnitude $\Delta q_0 = 100$. The linear solutions predicted at $q_0 = 100$ for the homogeneous plates by the 16-element meshes of the CPT and FSDT elements are $w(0) = 1.7578 \times 10^{-2}$ and $w(0) = 1.8292 \times 10^{-2}$, respectively. These agree with the analytical solutions (see Reddy [49])

$$w^{\text{CPT}}(0) = \frac{q_0 a^4}{64D} = 1.7578{\times}10^{-2}\,, \quad w^{\text{FSDT}}(0) = \frac{q_0 a^4}{64D}\left(1 + \frac{8}{3(1-\nu)K_s}\frac{h^2}{a^2}\right) = 1.8328{\times}10^{-2} \tag{65}$$

where $D = Eh^3/12(1-\nu^2)$. Many FSDT element are required to achieve the analytical solution. The corresponding nonlinear solutions are $w(0) = 1.7279 \times 10^{-2}$ and $w(0) = 1.7978 \times 10^{-2}$ (after three Newton iterations for a specified tolerance of $\epsilon = 10^{-3}$ for convergence).

The load parameter $P = (q_0 a^4/E_1 h^4)$ versus the dimensionless deflections $w(0)/h$ are presented in Fig. 3 for various values of the power-law index n and the ratio of the length scale to the plate thickness ℓ/h. In all cases, the effect of the material length scale entering through the couples stress term is to stiffen the clamped plate.

The next example deals with annular plates clamped at the outer edge and subjected to uniformly distributed transverse load of intensity q_0; the hole diameter is taken as $b = 0.25a$. The edge at $r = b$ is assumed to be free (i.e., no displacement boundary conditions are specified). The linear solutions predicted at $q_0 = 100$ for the homogeneous annular plates by the CPT and FSDT are $w(0.25) = 1.6296 \times 10^{-2}$ and $w(0.25) = 1.6850 \times 10^{-2}$, respectively; and for solid plates they are $w(0.25) = 1.5450 \times 10^{-2}$ and $w(0.25) = 1.6109 \times 10^{-2}$.

Plots of the load parameter $P = (q_0 a^4/E_1 h^4)$ versus dimensionless center deflection $w(0.25)/h$ are shown in Fig. 4 for $n = 0, 1, 5$ and $\ell/h = 0, 0.4$. For comparison, the results of solid circular (SC) plates are also included in the figure. The load-deflection curves for $\ell/h = 0.4$ run parallel to those with $\ell/h = 0$ (for any n). Solid plates carry more load than annular plates, but solid plates have more material (hence stiffer) than annular plates. Once again, we see the stiffening effect due to the inclusion of the length scale.

Next we consider annular plates clamped at the inner edge and subjected to uniformly distributed transverse load of intensity q_0; the hole diameter is taken as $b = 0.25a$. The edge at $r = a$ is assumed to be free (i.e., no displacement boundary conditions are specified). The linear solution predicted at $q_0 = 50$ by the CPT is $w(a) = 2.3586 \times 10^{-2}$ for $n = 0$ and $\ell/h = 0$; $w(a) = 1.8790 \times 10^{-2}$ for $n = 0$ and $\ell/h = 0.4$; $w(L) = 5.3324 \times 10^{-2}$

Figure 3

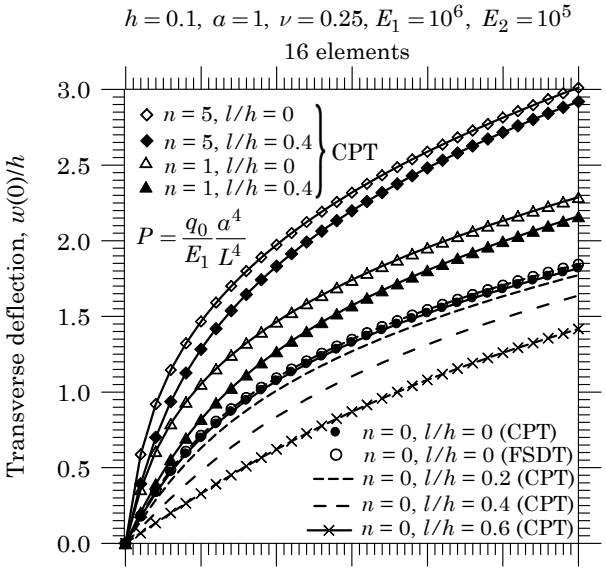

Figure 4

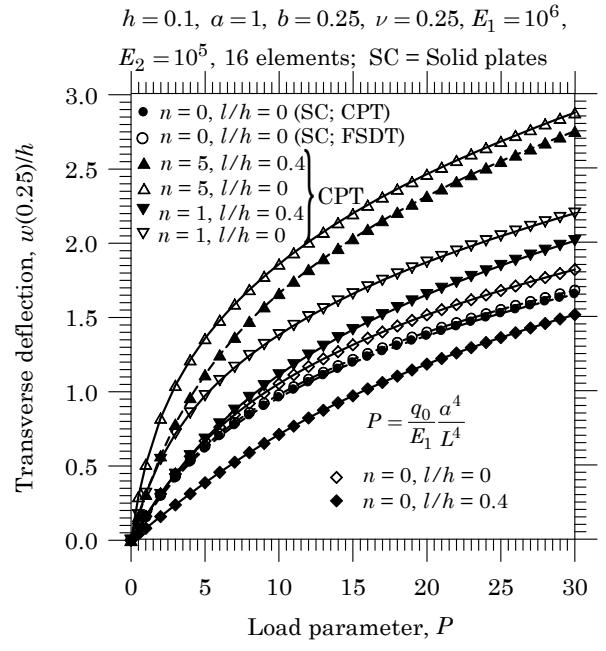

Fig. 4: Load-deflection curves for clamped annular plates for $n = 0, 1, 5$ and $l/h = 0, 0.4$.

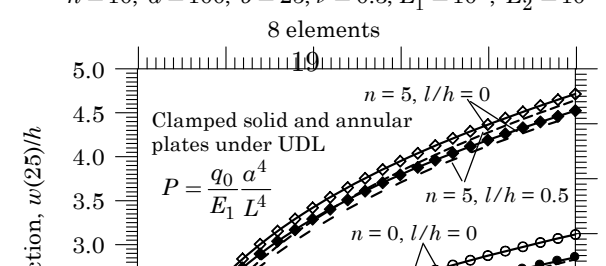

Figure 5

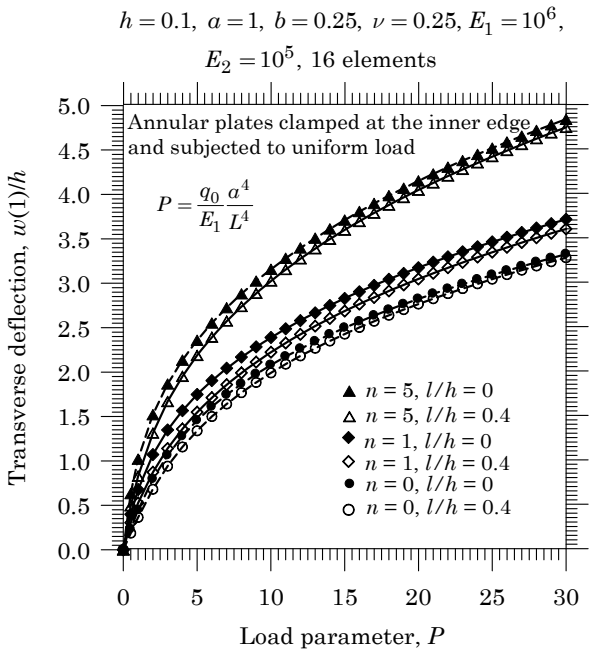

Fig. 5: Load-deflection curves for clamped annular plates for $n = 0, 1, 5$ and $l/h = 0, 0.4$.

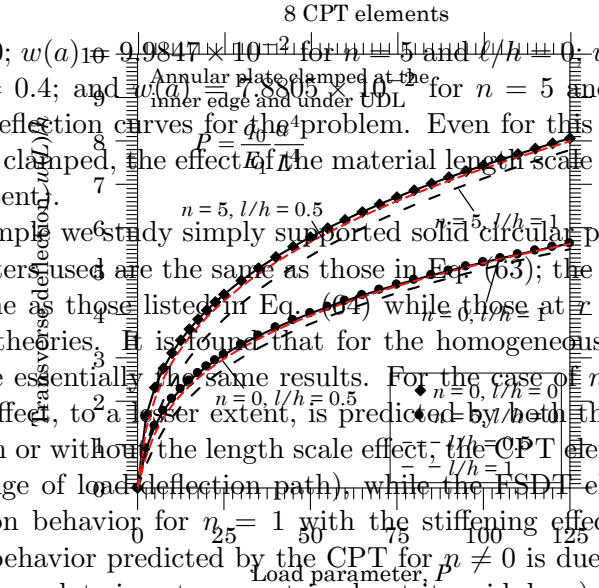

for $n = 1$ and $\ell/h = 0$; $w(a) = 9.9847 \times 10^{-2}$ for $n = 5$ and $\ell/h = 0$; $w(a) = 4.0893 \times 10^{-2}$ for $n = 1$ and $\ell/h = 0.4$; and $w(a) = 7.8805 \times 10^{-2}$ for $n = 5$ and $\ell/h = 0.4$. Figure 5 contains the load-deflection curves for the problem. Even for this cantilevered annular plate with inner edge clamped, the effect of the material length scale is to stiffen the plate (but for a smaller extent).

In the fourth example we study simply supported solid circular plates. The geometric and material parameters used are the same as those in Eq. (63); the boundary conditions at $r = 0$ are the same as those listed in Eq. (64) while those at $r = a$ are taken to be $u = w = 0$ in both theories. It is found that for the homogeneous case ($n = 0$), both CPT and FSDT gave essentially the same results. For the case of $n = 0$ and $\ell/h = 0.6$, again the stiffening effect, to a lesser extent, is predicted by both theories. However, for $n = 1$ and $n = 5$, with or without the length scale effect, the CPT element mesh predicted buckling (i.e., a change of load-deflection path), while the FSDT element mesh yielded smooth load-deflection behavior for $n = 1$ with the stiffening effect due to the length scale. The buckling behavior predicted by the CPT for $n \neq 0$ is due to the unsymmetric nature of the plate (i.e., plate is not symmetric about its midplane) as well as due to the restrictive kinematics (i.e., normality condition) that models the CPT plate stiffer than the FSDT. The effect of the length scale in the cases is to increase the buckling load. This phenomenon, that is, predicting softening behavior for buckled simply supported boundary conditions, is not reported for beams under mechanical loads. For $n = 0, 1, 5$ and $\ell/h = 0, 0.4, 0.6$, the sixteen-element mesh of the FSDT yielded convergent solutions and showed slight stiffening effect, as shown in Fig. 7.

Figure 6

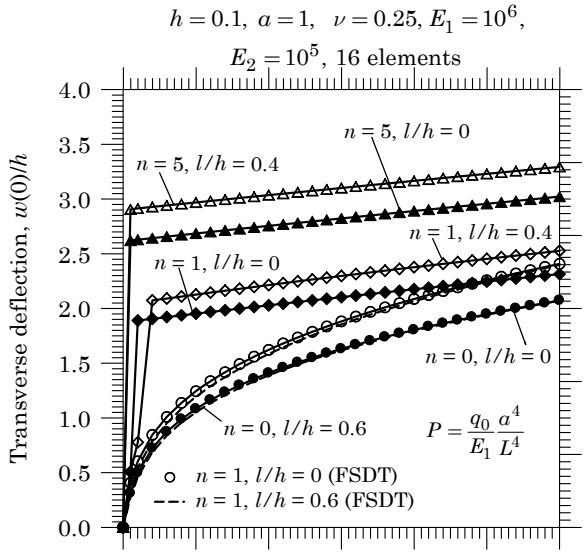

Figure 7

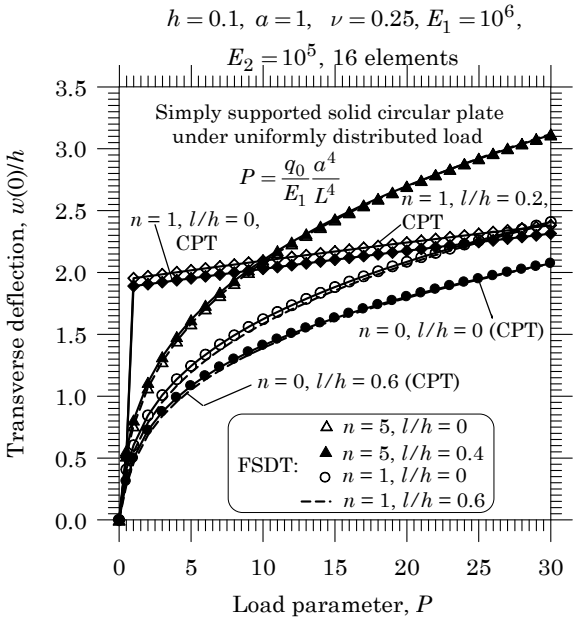

Fig. 7: Load-deflection curves for simply supported solid circular plates for $n = 0, 1, 5$ and $l/h = 0, 0.2, 0.4, 0.6$.

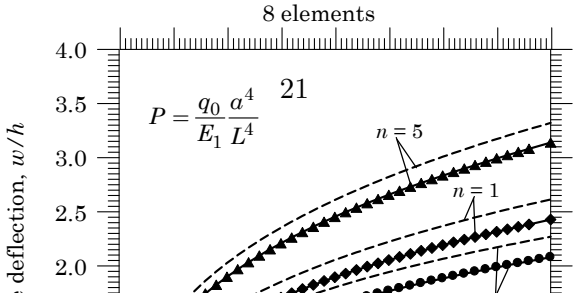

Figure 8

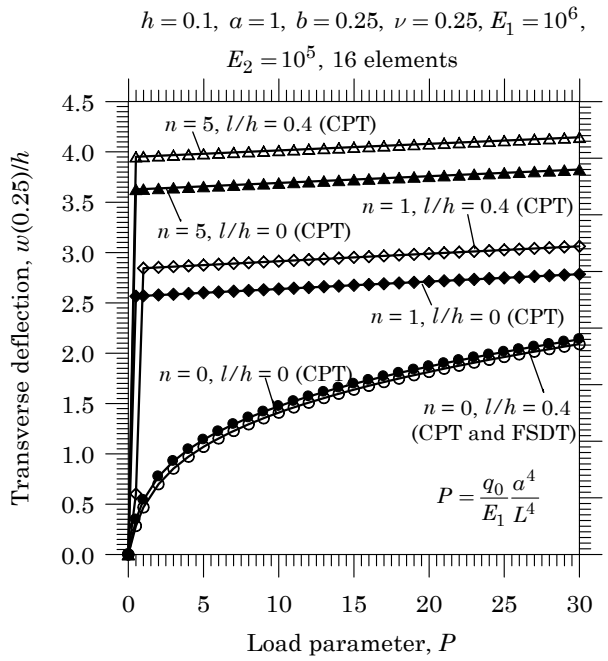

Fig. 8: Load-deflection curves for simply supported annular plates for $n = 0, 1, 5$ and $l/h = 0, 0.4$.

Finally, annular plates with simply supported outer edge are investigated. Figure 8 shows the load-deflection curves. Again, the CPT predicted buckling behavior while the FSDT did not even converge in most cases.

8 Summary and Conclusions

In this paper the classical (CPT) and first-order (FSDT) plate theories for axisymmetric bending of circular plates, accounting for through-thickness power-law variation of a two-constituent material, modified couple stress theory, and the von Kármán nonlinear strains are developed using Hamilton's principle. Then displacement finite element models for the transient analysis of both plate theories. Numerical results are presented for clamped solid circular and annular plates and also for simply supported solid circular plates, showing the effect of the power-law index and the ratio of the length scale parameter on the load-deflection behavior (static analysis). In the case of clamped plates, both theories yielded, for the geometric and material parameters selected, virtually the same results. The effect of the length scale is found to be that of stiffening the plates. However, for simply supported cases, the CPT element predicted buckling for $n \neq 0$, while the FSDT element exhibited smooth load-deflection behavior. Interestingly, the effect of the length scale for buckled circular plates is that of softening. This phenomena has not been reported in the literature and requires further study and validation by independent researchers.

Acknowledgments
The first author gratefully acknowledges the support of this work by the FidiPro Professorship from Aalto University (Finland) and Chair of Excellence from University Carlos III of Madrid (Spain). The second author acknowledges the support by the FidiPro project to Aalto University, while the third author gratefully acknowledges the support of the Chair of Excellence granted to the first author at University Carlos III of Madrid.

References

[1] M. Cadek, J.N. Coleman, K.P. Ryan, V. Nicolosi, G. Bister, A. Fonseca, J.B. Nagy, K. Szostak, F. Beguin, and W.J. Blau, Reinforcement of polymers with carbon nanotubes: the role of nanotube surface area, Nano Letters, 4 (2004) 353–356.

[2] M. Kaempgen, G.S. Duesberg, and S. Roth, Transparent carbon nanotube coatings, Applied Surface Science 252 (2005) 425–429.

[3] W.X. Chen, J.P. Tu, L.Y. Wang, H.Y. Gan, Z.D. Xu, and X.B. Zhang, Tribological application of carbon nanotubes in a metal-based composite coating and composites, Carbon 41 (2003) 215–222.

[4] R.D. Mindlin, Influence of couple-stresses on stress concentrations, Experimental Mechanics 3 (1963) 1–7.

[5] W.T. Koiter, Couple-stresses in the theory of elasticity: I and II, Koninklijke Nederlandse Akademie van Wetenschappen (Royal Netherlands Academy of Arts and Sciences) B67 (1964) 17–44.

[6] R.A. Toupin, Theories of elasticity with couple-stress, Archive for Rational Mechanics and Analysis 17 (1964) 85–112.

[7] R.D. Mindlin, Second gradient of strain and surface-tension in linear elasticity, International Journal of Solids and Structures 1 (1965) 217–238.

[8] F. Yang, A.C.M. Chong, D.C.C. Lam, and P. Tong, Couple stress based strain gradient theory for elasticity, International Journal of Solids and Structures 39 (2002) 2731–2743.

[9] D.C.C. Lam, F. Yang, A.C.M. Chong, J. Wang, and P. Tong, Experiments and theory in strain gradient elasticity, Journal of Mechanics and Physics of Solids 51 (2003), 1477–1508.

[10] A.R. Srinivasa and J.N. Reddy, A model for a constrained, finitely deforming, elastic solid with rotation gradient dependent strain energy, and its specialization to von Karman plates and beams, Journal of Mechanics and Physics of Solids 61 (2013) 873–885.

[11] J.N. Reddy and A.R. Srinivasa, Nonlinear theories of beams and plates accounting for moderate rotations and material length scales, International Journal of Non-Linear Mechanics (2014) in press.

[12] S.K. Park and X.L. Gao, Bernoulli-Euler beam model based on a modified couple stress theory, Journal of Micromechanics and Microengineering 16 (2006) 2355–2359.

[13] S.K. Park and X.L. Gao, Variational formulation of a modified couple stress theory and its application to a simple shear problem, Zeitschrift fr angewandte Mathematik

und Physik (ZAMP) 59 (2008) 904–917.
[14] H.M. Ma, X.L. Gao, J.N. Reddy, A microstructure-dependent Timoshenko beam model based on a modified couple stress theory. J Mech Phys Solids 56 (2008) 3379–3391.
[15] H.M. Ma, X.L. Gao, J.N. Reddy, A nonclassical Reddy-Levinson beam model based on a modified couple stress theory. Int J Multiscale Computational Engineering 8(2) (2010) 167–180.
[16] H.M. Ma, X.L. Gao, J.N. Reddy, A non-classical Mindlin plate model based on a modified couple stress theory. Acta Mechanica 220 (2011) 217–235.
[17] F. Yang, A.C.M. Chong, D.C.C. Lam, P. Tong, Couple stress based strain gradient theory for elasticity. Int. J. Solids Struct. 39 (2002) 2731–2743.
[18] J. Abdi, A. Koochi, A.S. Kazemi, and M. Abadyan, Modelling the effects of size dependence and dispersion forces on the pull-in instability of electrostatic cantilever NEMS using modified couple stress theory, Smart Materials and Structures, 20 (2011) 055011.
[19] B. Akgöz and Ö. Civalek, Strain gradient elasticity and modified couple stress models for buckling analysis of axially loaded micro-scaled beams, International Journal of Engineering Science 49 (2011) 1268-1280.
[20] M. Rahaeifard, M.H. Kharobaiyan, M. Asghari, and M.T. Ahmadian, Static pull-in analysis of microcantilevers based on the modified couple stress theory, Sensors and Actuators A 171 (2011) 370-374.
[21] R. Ansari, R. Gholami, and S. Sahmani, Free vibration analysis of size-dependent functionally graded microbeams based on the strain gradient Timoshenko beam theory, Composite Structures 94 (2011) 221-228.
[22] W. Xia, L. Wang, and L. Yin, Nonlinear non-classical microscale beams: static bending, postbuckling and free vibration, International Journal of Engineering Science 48 (2010) 2044-2053.
[23] M. Koizumi, The concept of FGM, Ceramic Transactions, Functionally Gradient Materials 34 (1993) 3–10.
[24] F. Erdogan, Fracture mechanics of functionally graded materials. Composites Engineering 5(1995) 753-770.
[25] G.N. Praveen, J.N. Reddy, Nonlinear transient thermoelastic analysis of functionally graded ceramic-metal plates, Journal of Solids and Structures 35(33) (1998) 4457–4476.
[26] J.N. Reddy, C.D. Chin, Thermomechanical analysis of functionally graded cylinders and plates, Journal of Thermal Stresses 26(1) (1998) 593–626.
[27] G.N. Praveen, C.D. Chin, J.N. Reddy, 'Thermoelastic analysis of functionally graded ceramic-metal cylinder, Journal of Engineering Mechanics, ASCE 125(11) (1999) 1259–1266.

[28] J.N. Reddy, Analysis of functionally graded plates, International Journal for Numerical Methods in Engineering 47 (2000) 663–684.
[29] J.N. Reddy, A general nonlinear third-order theory of functionally graded plates, International Journal of Aerospace and Lightweight Structures 1 (1) (2011) 1–21.
[30] J. Kim, G.H. Paulino, Finite element evaluation of mixed mode stress intensity factors in functionally graded materials, International Journal for Numerical Methods in Engineering 53 (2002) 1903–1935.
[31] Ch. Zhang, A. Savaidis, G. Savaidis, H. Zhu, Transient dynamic analysis of a cracked functionally graded material by a BIEM. Computational Materials Science 26 (2003) 167–174.
[32] C.F. Lü, C.W. Lim, and W.Q. Chen, Size-dependent elastic behavior of FGM ultra-thin films based on generalized refined theory, International Journal of Solids and Structures, 46 (2009) 1176-1185.
[33] M.H. Kahrobaiyan, M. Asghari, M. Rahaeifard, and M.T. Ahmadian, Investigation of the size-dependent dynamic characteristics of atomic force microscope microcantilevers based on the modified couple stress theory, International Journal of Engineering Science, 48 (2010) 1985-1994.
[34] J. Zhang and Y. Fu, Pull-in analysis of electrically actuated viscoelastic microbeams based on a modified couple stress theory, Meccanica 47 (2012) 1649-1658.
[35] B.S. Shariat, Y. Liu, and G. Rio, Modelling and experimental investigation of geometrically graded NiTi shape memory alloys, Smart Materials and Structures 22 (2013) 025030.
[36] J.N. Reddy, Microstructure-dependent couple stress theories of functionally graded beams, Journal of Mechanics and Physics of Solids 59 (2011) 2382–2399.
[37] J.N. Reddy, Jessica Berry, Modified couple stress theory of axisymmetric bending of functionally graded circular plates, Composites Structures 94 (2012) 3664–3668.
[38] A. Arbind, J.N. Reddy, Nonlinear analysis of functionally graded microstructure-dependent beams, Composite Structures, 98 (2013) 272–281.
[39] M. Simsek, J.N. Reddy, Bending and vibration of functionally graded microbeams using a new higher order beam theory and the modified couple stress theory, International Journal of Engineering Science 64 (2013) 37–53.
[40] M. Simsek, J.N. Reddy, A unified higher order beam theory for buckling of a functionally graded microbeam embedded in elastic medium using modified couple stress theory, Composite Structures 101 (2013) 47–58.
[41] J.N. Reddy, Jinseok Kim, A nonlinear modified couple stress-based third-order theory of functionally graded plates, Composite Structures 94 (2012) 1128–1143.
[42] J. Kim, J.N. Reddy, Analytical solutions for bending, vibration, and buckling of FGM plates using a couple stress-based third-order theory, Composite Structures 103 (2013) 8698.
[43] A. Arbind, J.N. Reddy, A. Srinivasa, Modified couple stress-based third-order theory for nonlinear analysis of functionally graded beams, Latin American Journal of Solids and Structures 11 (2014) 459–487.
[44] X. Li, B. Bhushan, K. Takashima, C.W. Baek, Y.K. Kim, Mechanical characterization of micro/nanoscale structures for MEMS/NEMS applications using nanoindentation

techniques. Ultramicroscopy 97 (2003) 481–494.
[45] J. Pei, F. Tian, T. Thundat, Glucose biosensor based on the microcantilever. Analytical Chem 76 (2004) 292–297.
[46] J.N. Reddy, Sami El-Borgi, and Jani Romanoff, Nonlinear analysis of functionally graded microbeams using eringen's nonlocal differential model. International Journal of Non-Linear Mechanics 67 (2014) 308318.
[47] J.N. Reddy, Energy Principles and Variational Methods in Applied Mechanics, 2nd ed., John Wiley & Sons, New York (2002).
[48] J.N. Reddy, Mechanics of Laminated Composite Plates and Shells, Theory and Analysis, 2nd ed., CRC Press, Boca Raton, FL (2004).
[49] J.N. Reddy, Theory and Analysis of Plates and Shells, 2nd ed., CRC Press, Boca Raton, FL (2007).
[50] J.N. Reddy, Introduction to Continuum Mechanics with Applications, Cambridge University Press, New York (2013).
[51] J.N. Reddy, An Introduction to the Finite Element Method, McGraw–Hill, New York (2006).
[52] J.N. Reddy, An Introduction to Nonlinear Finite Element Analysis, 2nd ed., Oxford University Press, Oxford, UK (2015).